REPORT DOCUMENTATION PAGE

Form Approved
OMB No. 0704-0188

PLEASE DO NOT RETURN YOUR FORM TO THE ABOVE ORGANIZATION.

1. REPORT DATE *(DD-MM-YYYY)*	2. REPORT TYPE	3. DATES COVERED *(From - To)*
11-10-2017	Journal Article	Aug 2016 - Oct 2016; Apr 2017-Sep 20

4. TITLE AND SUBTITLE
Optical polarization of excitons and trions under continuous and pulsed excitation in single layers of WSe2

5a. CONTRACT NUMBER
AOARD 14IOA018-134141

5b. GRANT NUMBER

5c. PROGRAM ELEMENT NUMBER

6. AUTHOR(S)
Hanbicki, Aubrey, T; Currie, Marc; Kioseoglou, George; Hellberg, Carl, Stephen; Friedman, Adam, L; Jonker, Berend, T

5d. PROJECT NUMBER

5e. TASK NUMBER

5f. WORK UNIT NUMBER

7. PERFORMING ORGANIZATION NAME(S) AND ADDRESS(ES)
Naval Research Laboratory, 4555 Overlook Ave. SW, Washington, DC 20375
University of Crete, Heraklion, Crete, 71003, Greece
Foundation for Research and Technology Hellas (FORTH), Heraklion, Crete, 71110, Greece

8. PERFORMING ORGANIZATION REPORT NUMBER

9. SPONSORING/MONITORING AGENCY NAME(S) AND ADDRESS(ES)
Naval Research Laboratory, 4555 Overlook Ave. SW, Washington, DC 20375

Air Force Office of Scientific Research, Wright-Patterson Air Force Base 5135 Pearson Road, Building 10,Wright-Patterson AFB, OH 45433

10. SPONSOR/MONITOR'S ACRONYM(S)
NRL, AFOSR

11. SPONSOR/MONITOR'S REPORT NUMBER(S)

12. DISTRIBUTION/AVAILABILITY STATEMENT

13. SUPPLEMENTARY NOTES

14. ABSTRACT

The potential for valleytronic operation has stimulated much interest in studying polarized emission from transition metal dichalcogenides. In most studies, however, little regard is given to the character of laser excitation. We measure the circularly polarized photoluminescence of WSe2 monolayers as a function of excitation energy for both continuous-wave (cw) and pulsed laser excitation sources. Using cw excitation, the temperature dependence of the depolarization of the trion follows the same trend as that of the neutral exciton and involves collisional broadening. However, the polarization of the trion is nearly twice the polarization of the neutral exciton at low temperatures. When a pulsed laser with the same average fluence is used as the excitation source, the degrees of polarization become very similar, in stark contrast to the cw results. The difference in polarization behaviors is linked to the different amounts of energy deposited in the system during these measurements for similar average fluences. At a moderate fluence, pulsed excitation also has the potential to fundamentally alter the emission characteristics of WSe2.

15. SUBJECT TERMS
Two-dimensional materials; photoluminescence; valley polarization; transition metal dichalcogenide

16. SECURITY CLASSIFICATION OF:			17. LIMITATION OF ABSTRACT	18. NUMBER OF PAGES	19a. NAME OF RESPONSIBLE PERSON
a. REPORT	b. ABSTRACT	c. THIS PAGE			Aubrey T. Hanbicki
U	U	U	UU	18	19b. TELEPHONE NUMBER *(Include area code)* (202) 767-3956

Reset

INSTRUCTIONS FOR COMPLETING SF 298

1. REPORT DATE. Full publication date, including day, month, if available. Must cite at least the year and be Year 2000 compliant, e.g. 30-06-1998; xx-06-1998; xx-xx-1998.

2. REPORT TYPE. State the type of report, such as final, technical, interim, memorandum, master's thesis, progress, quarterly, research, special, group study, etc.

3. DATES COVERED. Indicate the time during which the work was performed and the report was written, e.g., Jun 1997 - Jun 1998; 1-10 Jun 1996; May - Nov 1998; Nov 1998.

4. TITLE. Enter title and subtitle with volume number and part number, if applicable. On classified documents, enter the title classification in parentheses.

5a. CONTRACT NUMBER. Enter all contract numbers as they appear in the report, e.g. F33615-86-C-5169.

5b. GRANT NUMBER. Enter all grant numbers as they appear in the report, e.g. AFOSR-82-1234.

5c. PROGRAM ELEMENT NUMBER. Enter all program element numbers as they appear in the report, e.g. 61101A.

5d. PROJECT NUMBER. Enter all project numbers as they appear in the report, e.g. 1F665702D1257; ILIR.

5e. TASK NUMBER. Enter all task numbers as they appear in the report, e.g. 05; RF0330201; T4112.

5f. WORK UNIT NUMBER. Enter all work unit numbers as they appear in the report, e.g. 001; AFAPL30480105.

6. AUTHOR(S). Enter name(s) of person(s) responsible for writing the report, performing the research, or credited with the content of the report. The form of entry is the last name, first name, middle initial, and additional qualifiers separated by commas, e.g. Smith, Richard, J, Jr.

7. PERFORMING ORGANIZATION NAME(S) AND ADDRESS(ES). Self-explanatory.

8. PERFORMING ORGANIZATION REPORT NUMBER. Enter all unique alphanumeric report numbers assigned by the performing organization, e.g. BRL-1234; AFWL-TR-85-4017-Vol-21-PT-2.

9. SPONSORING/MONITORING AGENCY NAME(S) AND ADDRESS(ES). Enter the name and address of the organization(s) financially responsible for and monitoring the work.

10. SPONSOR/MONITOR'S ACRONYM(S). Enter, if available, e.g. BRL, ARDEC, NADC.

11. SPONSOR/MONITOR'S REPORT NUMBER(S). Enter report number as assigned by the sponsoring/ monitoring agency, if available, e.g. BRL-TR-829; -215.

12. DISTRIBUTION/AVAILABILITY STATEMENT. Use agency-mandated availability statements to indicate the public availability or distribution limitations of the report. If additional limitations/ restrictions or special markings are indicated, follow agency authorization procedures, e.g. RD/FRD, PROPIN, ITAR, etc. Include copyright information.

13. SUPPLEMENTARY NOTES. Enter information not included elsewhere such as: prepared in cooperation with; translation of; report supersedes; old edition number, etc.

14. ABSTRACT. A brief (approximately 200 words) factual summary of the most significant information.

15. SUBJECT TERMS. Key words or phrases identifying major concepts in the report.

16. SECURITY CLASSIFICATION. Enter security classification in accordance with security classification regulations, e.g. U, C, S, etc. If this form contains classified information, stamp classification level on the top and bottom of this page.

17. LIMITATION OF ABSTRACT. This block must be completed to assign a distribution limitation to the abstract. Enter UU (Unclassified Unlimited) or SAR (Same as Report). An entry in this block is necessary if the abstract is to be limited.

Nanoscale

PAPER

Cite this: *Nanoscale*, 2017, **9**, 17422

Optical polarization of excitons and trions under continuous and pulsed excitation in single layers of WSe_2†

A. T. Hanbicki,* [a] M. Currie,[b] G. Kioseoglou,[c,d] C. Stephen Hellberg,[a] A. L. Friedman[a] and B. T. Jonker[a]

Received 11th July 2017,
Accepted 11th October 2017

DOI: 10.1039/c7nr05019d

rsc.li/nanoscale

The potential for valleytronic operation has stimulated much interest in studying polarized emission from transition metal dichalcogenides. In most studies, however, little regard is given to the character of laser excitation. We measure the circularly polarized photoluminescence of WSe_2 monolayers as a function of excitation energy for both continuous-wave (cw) and pulsed laser excitation sources. Using cw excitation, the temperature dependence of the depolarization of the trion follows the same trend as that of the neutral exciton and involves collisional broadening. However, the polarization of the trion is nearly twice the polarization of the neutral exciton at low temperatures. When a pulsed laser with the same average fluence is used as the excitation source, the degrees of polarization become very similar, in stark contrast to the cw results. The difference in polarization behaviors is linked to the different amounts of energy deposited in the system during these measurements for similar average fluences. At a moderate fluence, pulsed excitation also has the potential to fundamentally alter the emission characteristics of WSe_2.

Introduction

Transition metal dichalcogenides (TMDs) such as WSe_2 and MoS_2 are a class of layered materials that can be easily isolated to single layers due to weak interlayer van der Waals bonding. As multilayers, these materials are indirect gap semiconductors. Single layers, however, because of their reduced dimensionality become direct-gap with a range of bandgaps in the visible region. Furthermore, because of large effective masses and reduced dielectric screening in these 2D systems, electrons and holes form strongly bound excitons due to the Coulomb interaction. Exciton binding energies on the order of 0.5 eV are predicted[1–4] and have been recently confirmed experimentally.[4–6] This leads to optical band gaps considerably lower in energy than the electronic band gaps. These and myriad other novel properties make TMDs suitable for applications in optoelectronics,[7–9] nonlinear optics,[10,11] and sensors.[12]

As in graphene, the hexagonal lattice of TMDs leads to non-equivalent *k*-points in the Brillouin zone. Furthermore, their broken inversion symmetry results in valley-contrasted optical selection rules for interband transitions. Therefore, the valley populations at the *K* and *K*′ points of the Brillioun zone are potential new state-variables of these systems.[13] In contrast to graphene, there is a large spin–orbit interaction in TMDs that leads to a unique coupling of carrier spin and *k*-space valley physics. It is therefore possible to explore intervalley scattering by taking advantage of the spin–valley coupling.[14,15] In practice, this can be done by independently populating and investigating the spin states in different *K*-valleys using circularly polarized light.

When a direct-gap TMD is excited with light of sufficient energy, electrons from the valence band are promoted to the conduction band and the resulting electron–hole pairs can form coulombic quasi-particles referred to as excitons. If the material is doped, the exciton can bind with an electron or a hole to form a charged exciton (trion). The radiative decay of these quasi-particles results in photoluminescence (PL) at energies characteristic of the material. By optically pumping a TMD with circularly polarized light and analyzing the subsequent PL for positive ($\sigma+$) and negative ($\sigma-$) helicity, it is possible to obtain some information on intervalley scattering.

[a]*Materials Science & Technology Division, Naval Research Laboratory, Washington, DC 20375, USA. E-mail: Hanbicki@nrl.navy.mil*
[b]*Optical Sciences Division, Naval Research Laboratory, Washington, DC 20375, USA*
[c]*Dept. of Materials Science and Technology, Univ. of Crete, Heraklion, Crete, 71003, Greece*
[d]*Institute of Electronic Structure and Laser (IESL), Foundation for Research and Technology Hellas (FORTH), Heraklion, Crete, 71110, Greece*

†Electronic supplementary information (ESI) available: Raman spectrum of our WSe_2 sample, differential reflectivity, power dependence spectra, an alternate fitting scheme, raw helicity analyzed photoluminescence spectra and summary of peak intensities, and derivation of polarization based on rate equations. See DOI: 10.1039/c7nr05019d

This property has been exploited to great effect in MoS_2[16–19] and WS_2,[20–22] and to some extent in $MoSe_2$[23,24] and WSe_2.[25,26] Various depolarization mechanisms have been proposed, including phonon-mediated intervalley scattering,[18,23,27] exciton scattering either directly or through an intermediate *k*-point with a spin flip-flop,[28] exchange interaction enabled depolarization,[29–31] and a D'yakonov-Perel' like mechanism.[32]

In this study, we measure and compare the circularly polarized PL of WSe_2 monolayers as a function of excitation energy using both continuous-wave (cw) lasers and pulsed lasers. Both types of excitation sources are used in the literature, often interchangeably. We find that with cw excitation, the polarization of the trion is nearly twice the polarization of the neutral exciton at 5 K, and the temperature dependence of the polarized emission from the neutral exciton and the trion is similar. In contrast, with pulsed laser excitation, the degrees of polarization of the neutral and charged excitons are nearly equal for a similar average fluence. We attribute the difference to processes that are enabled by the large amount of energy deposited during the pulsed excitation, specifically non-radiative processes such as Auger recombination. We also found that the emission characteristics of WSe_2 can be fundamentally altered with pulsed laser excitation.

Experimental details

The WSe_2 samples used in this study were mechanically exfoliated from bulk crystals and deposited onto a 275 nm SiO_2 layer on a Si substrate, as shown in the inset of Fig. 1a. Monolayer regions are typically 5–10 μm across and were identified using an optical microscope and confirmed with Raman spectroscopy at room temperature and 488 nm excitation (see the ESI, Fig. S1†).[33] The photoluminescence data were taken for a backscattering geometry using a micro-PL setup (spatial resolution of 1 μm) with a 50× objective and incorporating a continuous-flow He-cryostat. The samples were excited with either cw solid-state lasers of various fixed wavelengths or a tunable pulsed laser. The pulsed source was a Ti: sapphire pumped, optical parametric amplifier tunable from 1.77 to 2.48 eV (700–500 nm) with a typical pulse width of 100 fs, and operating at a 250 kHz repetition rate. A scanning monochromator was used to reduce the spectral bandwidth to <5 meV (1 nm). The PL emission was collected, passed through a polarization analyzer composed of a quarter-wave plate and a linear polarizer, dispersed using a spectrograph, and detected using a charge coupled device (CCD) camera.

Results and discussion

Cw excitation

Fig. 1a shows the PL spectra of exfoliated WSe_2 for several excitation energies (E_{exc} = 1.89, 1.96, and 2.33 eV) measured at 5 K. These spectra are obtained after excitation with positive helicity light and were analyzed for positive (σ+, solid red line) and negative (σ–, dotted blue line) helicity. In these PL spectra, there are several spectral features including a neutral exciton, X^0 at 1.75 eV, a charged exciton, X^T at 1.72 eV, and a prominent emission feature L at 1.66 eV. The temperature dependence of the photoluminescence taken with an excitation energy of 1.96 eV is shown in Fig. 1b for temperatures 5 K, 50 K and 100 K. These spectra are normalized to the X^0 intensity. While the X^0 and X^T emission channels clearly survive at temperatures above 100 K, the L feature is quickly quenched. Similar to other studies, we attribute this feature to localized excitons.[30,34,35] While the focus of this report will be on the polar-

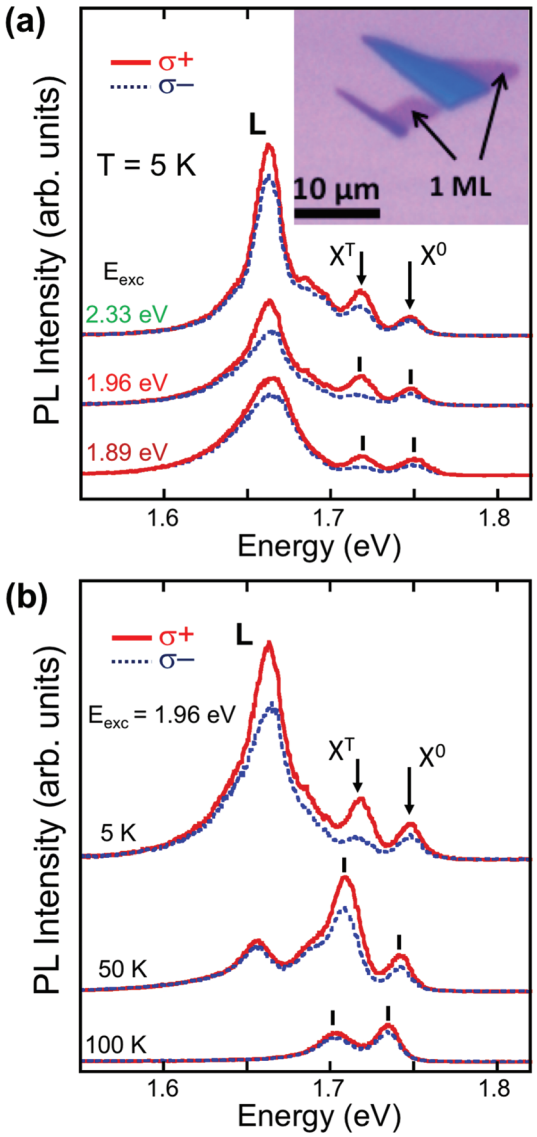

Fig. 1 (a) PL spectra at T = 5 K analyzed for σ+ and σ– at 3 different photo-excitation energies: 1.89 eV, 1.96 eV, and 2.33 eV. Emission from the neutral (X^0) and charged (X^T) excitons, as well as a localized exciton (L), is identified. The data are normalized and offset for clarity. Inset: Optical image of the WSe2 single layer. (b) PL spectra at an excitation energy of 1.96 eV analyzed for σ+ and σ– at 3 different temperatures: 5 K, 50 K, and 100 K. Note the expected shift of the features as a function of temperature.

ization of the two highest energy features, X^0 and X^T, for reference we include in the ESI† additional data on this sample including differential reflectivity (Fig. S2†) and power dependence spectra obtained with cw excitation (Fig. S3†). We note that the emission and absorption energies we measured are in good agreement with other theoretical and experimental characterization of WSe_2 (ESI Table 1†).

A summary of the circularly polarized emission of X^0 and X^T as a function of temperature is shown in Fig. 2. The degree of circular polarization of the PL is defined as

$$P_{\text{circ}} = (I_+ - I_-)/(I_+ + I_-), \quad (1)$$

where I_+ (I_-) is the PL intensity of the $\sigma+$ ($\sigma-$) component. In this figure, the symbols are data points and the solid lines are fits to the data as discussed below. For the neutral exciton (shown in Fig. 2a), the degree of circular polarization is roughly constant up to 30 K after which it rapidly decreases. The low temperature behavior is consistent with reports based on the Kerr rotation of WSe_2 [30] where it was shown that the valley relaxation time has little temperature dependence until 30 K. The trion (shown in Fig. 2b) has a much higher initial degree of polarization than the neutral exciton, and the polarization exhibits a much stronger temperature dependence. Even for relatively high excitation energies, the depolarization of X^T is much more rapid with increasing temperature than that of X^0, as shown for 2.33 eV excitation in the inset of Fig. 2b. For both X^0 and X^T, no polarization remains above 200 K. From these data, it is clear that the trion has nearly twice the degree of circularly polarized emission of X^0 at 5 K. Other studies report similar behavior in both WSe_2 [26] as well as WS_2;[20,30] however, this observation has received little attention.

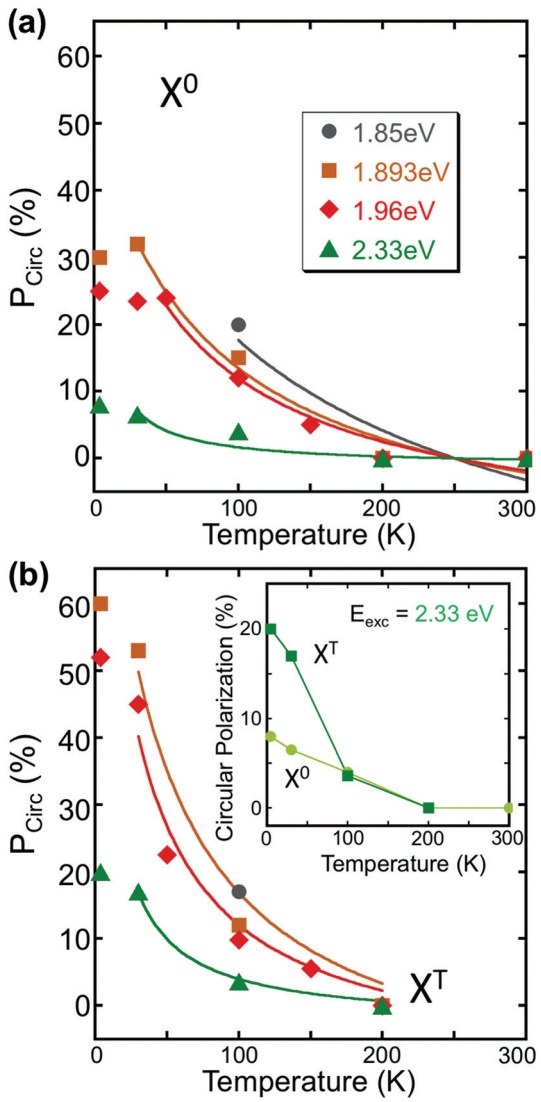

Fig. 2 Temperature dependence of the circular polarization of the (a) neutral exciton, X^0, and (b) charged exciton, X^T, for different excitation energies. Symbols are data and lines are fits described in the text. Inset: Comparison of the circular polarization data for X^0 and X^T as a function of temperature with 2.33 eV excitation.

To understand the temperature dependent depolarization behavior observed with cw excitation we use a rate equation framework. For steady-state conditions the circularly polarized emission of a TMD can be expressed as

$$P_{\text{circ}} = \frac{P_0}{1 + 2\frac{\tau_r}{\tau_v}}, \quad (2)$$

where τ_r is the exciton recombination time, τ_v is the intervalley scattering time, and P_0 is the initial polarization.[16,18] Based on a theoretical treatment presented in the literature, we assume that the exciton recombination has the temperature dependence $\tau_r = \gamma_1 T$.[36] This functional form has also been observed for 2D semiconductor quantum well systems.[37,38] For intervalley scattering it has been shown that, in low-doped samples at elevated temperatures, thermal broadening is the main mechanism and valley relaxation is proportional to the inverse of temperature, $\tau_v = \gamma_2/T$.[29,30,39] When considering sufficiently doped samples, however, collisional broadening becomes important and $\tau_v \sim (1 - \gamma_2 T)$.[39] As we will discuss, the latter of these two functional forms better fits our data.

On including the appropriate temperature dependence, eqn (2) becomes,

$$P_{\text{circ}} = \frac{P_0}{1 + 2\frac{\gamma_1 T}{1 - \gamma_2 T}}, \quad (3)$$

Eqn (3) is used for the fits shown in Fig. 2. In these fits we set $\gamma_2 = 0.004\ \text{K}^{-1}$ based on the predictions of linewidth broadening in ref. 39. For X^0 and X^T we use $P_0(X^T) = 100\%$ and $P_0(X^0) = 50\%$ based on the fact that X^T has double the initial polarization of X^0 (as discussed earlier). Therefore, the only free fitting parameter is γ_1. This functional form recreates the general trends seen in the temperature dependence of our data. Fits where only thermal broadening is considered are presented in the ESI (Fig. S2 and S3†) and are clearly insufficient. In our parameterization, γ_2 contains contributions from many different physical parameters such as lattice constant, exciton binding energy, electronic band gap, and exciton

effective mass. Again, also implicit in the functional form of τ_v are a doped sample and collisional broadening.[39] This is consistent with our observation of the charged exciton in PL, as well as the prominence of the peak associated with localized emission.

Pulsed excitation

Excitation with a pulsed laser results in remarkably different photoluminescence from that for WSe_2 and impacts subsequent cw-excited PL as well. Fig. 3a shows a sequence of PL spectra taken with a cw excitation of 1.96 eV at 5 K. For the top spectrum (green, "before"), the sample was not exposed to a pulsed laser and is similar to the spectra in Fig. 1. After acquiring this spectrum, the sample was exposed to a pulsed laser with an energy of 2.1 eV (590 nm) and an average power of ~35 μW (fluence ~1 mJ cm^{-2}) for ~10 seconds. Another spectrum was then immediately acquired under the same cw laser excitation conditions and the spectrum was fundamentally altered. This is shown in the middle spectrum of Fig. 3a (red, "after"). Note that, all of the spectral features collapse to a single emission peak at 1.689 eV. This spectral condition persisted for >10 min at a low temperature. When the sample was warmed up to room temperature, *in situ* and again cooled to 5 K, the original features were recovered using the same cw excitation conditions (Fig. 3a, black, "recovery"). Similar phenomena were reported for MoS_2,[40] $MoSe_2$,[40] and WS_2 [41] where the spectra underwent a fundamental change after laser exposure. In the case of WS_2, the PL spectral changes could be affected by both pulsed and cw laser excitation.[41] The emission channel of the modified WSe_2 sample is of indeterminate origin but could be due to emission from an exciton bound to an ionized impurity.[42] Based on Fig. 3a, it is clear that exposing the sample to a pulsed laser with even moderate power will result in strongly modified PL. Therefore, care must be taken when studying PL from X^0 and X^T with a pulsed excitation. Specifically, sufficiently low power levels must be employed to avoid conditioning the sample into an indeterminate state. Whenever the sample PL characteristics are modified, *e.g.*, with too much power from the excitation source, however, they can be recovered by cycling to room temperature and back. Indeed, we discover the overall range of powers in which PL is accessible when the pulsed laser is very small. To observe any PL with the pulsed laser, the average power required is on the same scale as the lower end of the cw power used (see ESI Fig. S4†). When the power is increased, however, the pulsed laser starts modifying the emission character with only small increases in power. Although the average power of the pulsed laser is about the same as the cw laser, the instantaneous energy imparted to the system is much larger with the pulsed laser, and modifications to the system ensue.

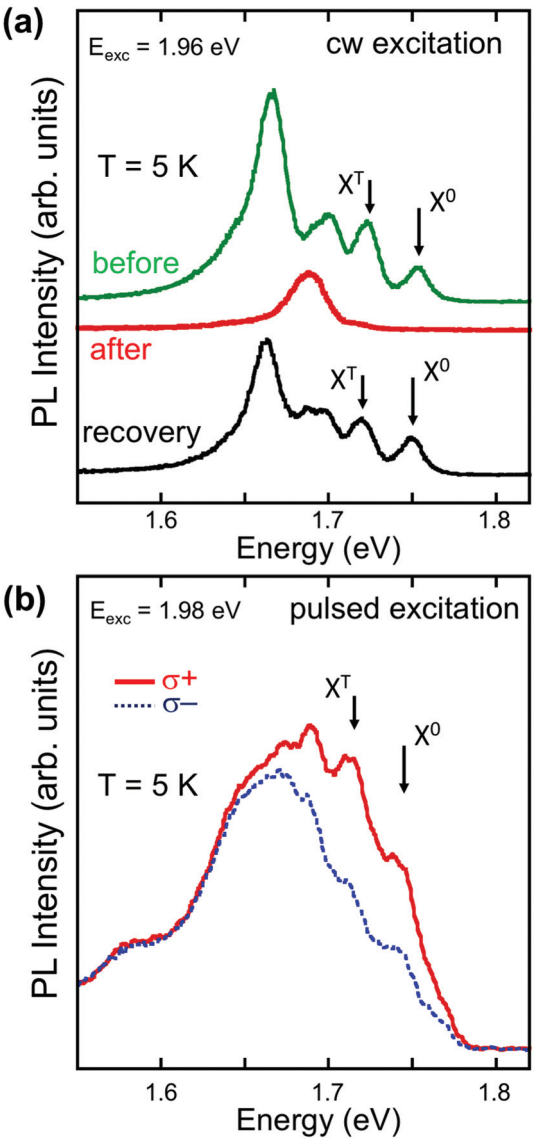

Fig. 3 (a) Three PL spectra measured with cw excitation at T = 5 K and a power of 40 μW, with no analysis of polarization. The top spectrum (green) is recorded before and the middle spectrum (red) is recorded after the "conditioning" of the sample with a pulsed laser. The bottom spectrum (black) is recorded after the sample is warmed to 300 K after conditioning. (b) PL spectra using a pulsed photoexcitation energy of 1.977 eV and an average power of 40 μW taken at T = 5 K analyzed for $\sigma+$ and $\sigma-$. Emission from the neutral (X^0) and charged (X^T) excitons is identified on both panels.

Regardless of the pulsed laser power, the qualitative characters of the emission are significantly different between pulsed and cw excitation. Fig. 3b shows the PL spectra taken at 5 K with a pulsed excitation energy of 1.98 eV, an average power of <20 μW and analyzed for $\sigma+$ and $\sigma-$. As before, it is possible to resolve the X^0 and X^T emission. But now instead of a well-resolved, dominant L peak at 1.66 eV, there is a broad background at 1.68 eV. Again, because of the indeterminate nature of this feature, we confine our discussion to the neutral exciton and trion. In the ESI,† we present the helicity resolved spectra for all of the excitation conditions we measured, Fig. S4–S6.† We note here that the PL intensities of X^0 and X^T under pulsed excitation are almost 10 times lower than the intensity under cw conditions for similar average beam powers, Fig. S7.†

Polarization *vs.* excitation energy

Fig. 4 summarizes the circular polarization as a function of excitation energy at 5 K for excitation with cw (Fig. 4a) and pulsed sources (Fig. 4b). The solid symbols indicate X^0 emission and the open symbols indicate X^T emission. As the excitation energy is increased, the polarized emission generally decreases. This trend has been seen in MoS_2 and $MoSe_2$ and can be understood as an increase in phonon-mediated intervalley scattering enabled by an increase of excess energy in the system above the material dependent threshold necessary for phonon generation[18,23,27] or by the electron–hole exchange interaction.[29,31]

The trion polarization using cw excitation falls in the region indicated in the yellow band in Fig. 4. As shown in Fig. 4(a), and previously noted, the trion, X^T, exhibits twice the degree of circularly polarized emission as that of the neutral exciton, X^0. Unexpectedly, under pulsed excitation, Fig. 4(b), both X^0 and X^T have the same circularly polarized emission which falls in the same region as X^T polarization under cw conditions. There is some deviation from this behavior at very low and very high excitation energies, but the factor of 2 observed between the polarization of X^0 and X^T with cw excitation is not apparent for pulsed excitation.

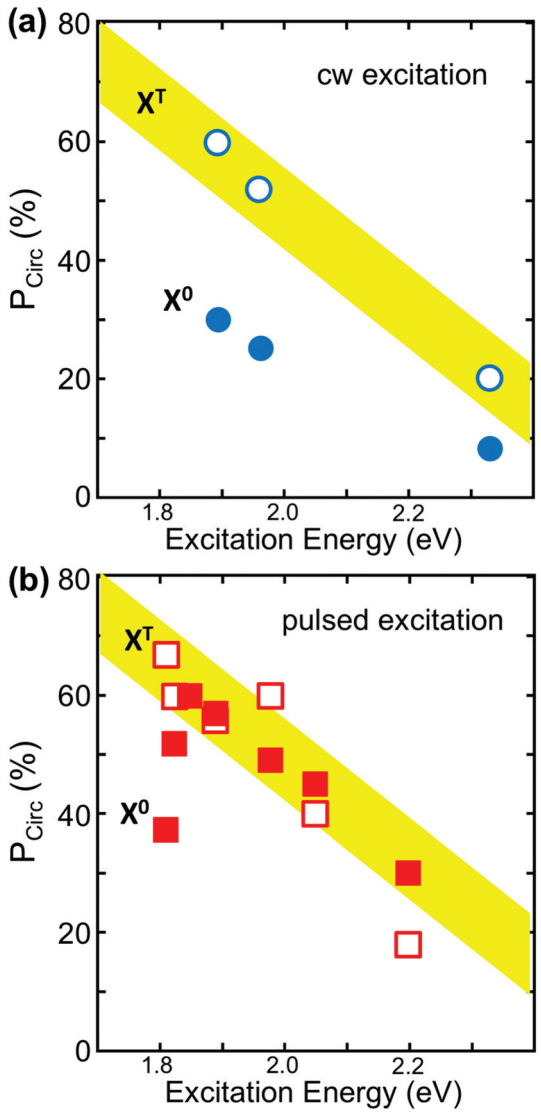

Fig. 4 A summary of circular polarization measured at the trion (open symbols) and neutral exciton (closed symbols) emission energies is shown as a function of excitation energy for (a) cw excitation and (b) pulsed excitation at 5 K. The yellow band is a guide to the eye.

Changes in polarization are usually a consequence of changes in either the valley relaxation time or the exciton recombination time, as shown in eqn (2). To understand our observed behavior, we recast this equation in terms of recombination rates. As described in the ESI† and elsewhere,[20] the polarization can be described by

$$P_{\mathrm{circ}} = \frac{P_0}{1 + 2\beta/(\alpha + A)}, \quad (4)$$

where α is the radiative recombination rate, A is the non-radiative recombination rate, and β is the valley relaxation rate. Under cw excitation, the density of free carriers is low and we expect non-radiative contributions such as Auger recombination to be small. The valley relaxation time is longer for the trion than for the exciton, *i.e.* $\beta_{X^0} > \beta_{X^T}$.[43] Thus for cw excitation we expect $P_{\mathrm{circ}}(X^0) < P_{\mathrm{circ}}(X^T)$. Under pulsed excitation, the density of free carriers surrounding the excitons and trions is higher which enhances non-radiative Auger recombination. Indeed, as discussed the measured PL intensities of both excitons and trions are nearly 10 times lower with pulsed excitation compared to cw excitation for similar average powers (Fig. S7†). With a large non-radiative recombination rate A, we can then expect $P_{\mathrm{circ}}(X^0) \sim P_{\mathrm{circ}}(X^T)$, as observed.

Conclusions

In this study, we compared the measured circular polarization of WSe_2 monolayers for excitation with both cw and pulsed lasers with similar average fluences. Both excitation types are commonly used, often interchangeably, for studies of intervalley scattering in TMDs. For cw excitation, the temperature dependence of the polarization for the neutral exciton and trion are similar; however the initial polarization of the trion is significantly larger. We demonstrate that collisional broadening is a primary mechanism in the valley scattering process producing the depolarization as a function of temperature. When pulsed laser excitation is used however, the polarization behaviors of the neutral and charged excitons become similar, indicating that the pulsed laser interacts with the material differently. The pulsed laser also has the potential to fundamentally change the emission characteristics of WSe_2 and hence must be used judiciously. Understanding the polarization behavior of WSe_2 under various conditions is an enabling step to utilizing the valleytronic functionality of this material.

Conflicts of interest

There are no conflicts to declare.

Acknowledgements

GK gratefully acknowledges the hospitality and support of the Naval Research Laboratory where the experiments were performed. This work was supported by core programs at NRL and the NRL Nanoscience Institute, and by the Air Force Office of Scientific Research under contract number AOARD 14IOA018-134141.

Notes and references

1 T. Cheiwchanchamnangij and W. R. L. Lambrecht, *Phys. Rev. B: Condens. Matter*, 2012, **85**, 205302.
2 H.-P. Komsa and A. V. Krasheninnikov, *Phys. Rev. B: Condens. Matter*, 2012, **86**, 241201.
3 D. Y. Qiu, F. H. da Jornada and S. G. Louie, *Phys. Rev. Lett.*, 2013, **111**, 216805.
4 Z. Ye, T. Cao, K. O'Brien, H. Zhu, X. Yin, Y. Wang, S. G. Louie and X. Zhang, *Nature*, 2014, **513**, 214–218.
5 A. T. Hanbicki, M. Currie, G. Kioseoglou, A. L. Friedman and B. T. Jonker, *Solid State Commun.*, 2015, **203**, 16–20.
6 G. Wang, X. Marie, I. Gerber, T. Amand, D. Lagarde, L. Bouet, M. Vidal, A. Balocchi and B. Urbaszek, *Phys. Rev. Lett.*, 2015, **114**, 97403.
7 D. Akinwande, N. Petrone and J. Hone, *Nat. Commun.*, 2014, **5**, 5678.
8 Q. H. Wang, K. Kalantar-Zadeh, A. Kis, J. N. Coleman and M. S. Strano, *Nat. Nanotechnol.*, 2012, **7**, 699–712.
9 S. Z. Butler, S. M. Hollen, L. Cao, Y. Cui, J. A. Gupta, H. R. Gutiérrez, T. F. Heinz, S. S. Hong, J. Huang, A. F. Ismach, E. Johnston-Halperin, M. Kuno, V. V. Plashnitsa, R. D. Robinson, R. S. Ruoff, S. Salahuddin, J. Shan, L. Shi, M. G. Spencer, M. Terrones, W. Windl and J. E. Goldberger, *ACS Nano*, 2013, **7**, 2898–2926.
10 X. Yin, Z. Ye, D. A. Chenet, Y. Ye, K. O'Brien, J. C. Hone and X. Zhang, *Science*, 2014, **344**, 488–490.
11 D. Li, W. Xiong, L. Jiang, Z. Xiao, H. Rabiee Golgir, M. Wang, X. Huang, Y. Zhou, Z. Lin, J. Song, S. Ducharme, L. Jiang, J.-F. Silvain and Y. Lu, *ACS Nano*, 2016, **10**, 3766–3775.
12 F. K. Perkins, A. L. Friedman, E. Cobas, P. M. Campbell, G. G. Jernigan and B. T. Jonker, *Nano Lett.*, 2013, **13**, 668–673.
13 A. Rycerz, J. Tworzydło and C. W. J. Beenakker, *Nat. Phys.*, 2007, **3**, 172–175.
14 D. Xiao, G.-B. Liu, W. Feng, X. Xu and W. Yao, *Phys. Rev. Lett.*, 2012, **108**, 196802.
15 X. Xu, W. Yao, D. Xiao and T. F. Heinz, *Nat. Phys.*, 2014, **10**, 343–350.
16 K. F. Mak, K. He, J. Shan and T. F. Heinz, *Nat. Nanotechnol.*, 2012, **7**, 494–498.
17 T. Cao, G. Wang, W. Han, H. Ye, C. Zhu, J. Shi, Q. Niu, P. Tan, E. Wang, B. Liu and J. Feng, *Nat. Commun.*, 2012, **3**, 887.
18 G. Kioseoglou, A. T. Hanbicki, M. Currie, A. L. Friedman, D. Gunlycke and B. T. Jonker, *Appl. Phys. Lett.*, 2012, **101**, 221907.
19 G. Sallen, L. Bouet, X. Marie, G. Wang, C. R. Zhu, W. P. Han, Y. Lu, P. H. Tan, T. Amand, B. L. Liu and B. Urbaszek, *Phys. Rev. B: Condens. Matter*, 2012, **86**, 81301.
20 A. T. Hanbicki, G. Kioseoglou, M. Currie, C. S. Hellberg, K. M. McCreary, A. L. Friedman and B. T. Jonker, *Sci. Rep.*, 2016, **6**, 18885.
21 A. T. Hanbicki, K. M. McCreary, G. Kioseoglou, M. Currie, C. S. Hellberg, A. L. Friedman and B. T. Jonker, *AIP Adv.*, 2016, **6**, 55804.
22 G. Plechinger, P. Nagler, A. Arora, R. Schmidt, A. Chernikov, A. G. del Águila, P. C. M. Christianen, R. Bratschitsch, C. Schüller and T. Korn, *Nat. Commun.*, 2016, **7**, 12715.
23 G. Kioseoglou, A. T. Hanbicki, M. Currie, A. L. Friedman and B. T. Jonker, *Sci. Rep.*, 2016, **6**, 25041.
24 G. Wang, E. Palleau, T. Amand, S. Tongay, X. Marie and B. Urbaszek, *Appl. Phys. Lett.*, 2015, **106**, 112101.
25 A. M. Jones, H. Yu, N. J. Ghimire, S. Wu, G. Aivazian, J. S. Ross, B. Zhao, J. Yan, D. G. Mandrus, D. Xiao, W. Yao and X. Xu, *Nat. Nanotechnol.*, 2013, **8**, 634–638.
26 A. M. Jones, H. Yu, J. R. Schaibley, J. Yan, D. G. Mandrus, T. Taniguchi, K. Watanabe, H. Dery, W. Yao and X. Xu, *Nat. Phys.*, 2016, **12**, 323–327.
27 B. R. Carvalho, Y. Wang, S. Mignuzzi, D. Roy, M. Terrones, C. Fantini, V. H. Crespi, L. M. Malard and M. A. Pimenta, *Nat. Commun.*, 2017, **8**, 14670.
28 C. Mai, A. Barrette, Y. Yu, Y. G. Semenov, K. W. Kim, L. Cao and K. Gundogdu, *Nano Lett.*, 2014, **14**, 202–206.
29 M. M. Glazov, E. L. Ivchenko, G. Wang, T. Amand, X. Marie, B. Urbaszek and B. L. Liu, *Phys. Status Solidi B*, 2015, **252**, 2349–2362.
30 C. R. Zhu, K. Zhang, M. Glazov, B. Urbaszek, T. Amand, Z. W. Ji, B. L. Liu and X. Marie, *Phys. Rev. B: Condens. Matter*, 2014, **90**, 161302(R).
31 M. Baranowski, A. Surrente, D. K. Maude, M. Ballottin, A. A. Mitioglu, P. C. M. Christianen, Y. C. Kung, D. Dumcenco, A. Kis and P. Plochocka, *2D Mater.*, 2017, **4**, 25016.
32 T. Yan, X. Qiao, P. Tan and X. Zhang, *Sci. Rep.*, 2015, **5**, 15625.
33 H. Sahin, S. Tongay, S. Horzum, W. Fan, J. Zhou, J. Li, J. Wu and F. M. Peeters, *Phys. Rev. B: Condens. Matter*, 2013, **87**, 165409.
34 Y. You, X.-X. Zhang, T. C. Berkelbach, M. S. Hybertsen, D. R. Reichman and T. F. Heinz, *Nat. Phys.*, 2015, **11**, 477–481.
35 G. Wang, L. Bouet, D. Lagarde, M. Vidal, A. Balocchi, T. Amand, X. Marie and B. Urbaszek, *Phys. Rev. B: Condens. Matter*, 2014, **90**, 075413.

36 M. Palummo, M. Bernardi and J. C. Grossman, *Nano Lett.*, 2015, **15**, 2794–2800.
37 L. C. Andreani, F. Tassone and F. Bassani, *Solid State Commun.*, 1991, **77**, 641–645.
38 D. S. Citrin, *Solid State Commun.*, 1992, **84**, 281–284.
39 S. Konabe, *Appl. Phys. Lett.*, 2016, **109**, 73104.
40 F. Cadiz, C. Robert, G. Wang, W. Kong, X. Fan, M. Blei, D. Lagarde, M. Gay, M. Manca, T. Taniguchi, K. Watanabe, T. Amand, X. Marie, P. Renucci, S. Tongay and B. Urbaszek, *2D Mater.*, 2016, **3**, 45008.
41 M. Currie, A. T. Hanbicki, G. Kioseoglou and B. T. Jonker, *Appl. Phys. Lett.*, 2015, **106**, 201907.
42 E. H. Bogardus and H. B. Bebb, *Phys. Rev.*, 1968, **176**, 993–1002.
43 A. Singh, K. Tran, M. Kolarczik, J. Seifert, Y. Wang, K. Hao, D. Pleskot, N. M. Gabor, S. Helmrich, N. Owschimikow, U. Woggon and X. Li, *Phys. Rev. Lett.*, 2016, **117**, 257402.

Optical polarization of excitons and trions under continuous and pulsed excitation in single layers of WSe_2

A.T. Hanbicki[a], M. Currie[b], G. Kioseoglou[c,d], C.S. Hellberg[a], A.L. Friedman[a], and B.T. Jonker[a]

[a] *Materials Science & Technology Division*, *Naval Research Laboratory*, Washington, DC 20375

[b] *Optical Sciences Division, Naval Research Laboratory*, Washington, DC 20375

[c] *Dept. of Materials Science and Technology, Univ. of Crete, Heraklion Crete, 71003, Greece*

[d] *Institute of Electronic Structure and Laser (IESL), Foundation for Research and Technology Hellas (FORTH), Heraklion Crete, 71110, Greece*

SUPPLEMENTARY INFORMATION

Section 1: **Raman of WSe_2**

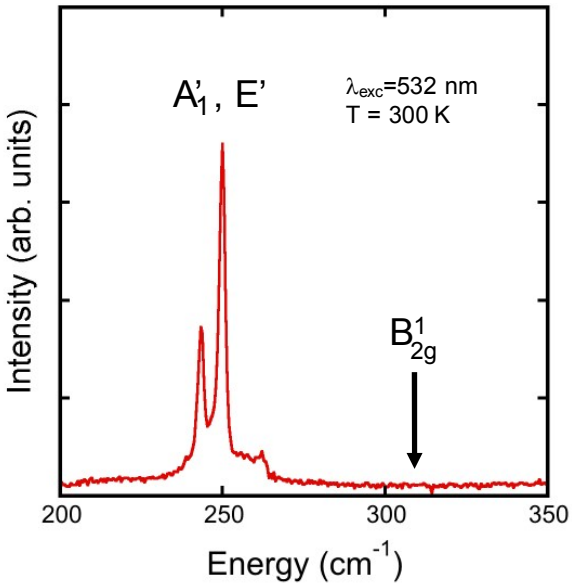

Fig. S1 – Raman spectrum of WSe_2 taken at room temperature with an excitation of 532 nm. The splitting of the A'_1 and E' peak near 252 cm^{-1} is consistent with a small amount of uniaxial strain in the system.[1] For multilayer material, a B^1_{2g} peak is expected at 309 cm^{-1}, therefore an absence of this peak is consistent with single layer material.[2]

Section 2: **Differential Reflectivity/Absorption**

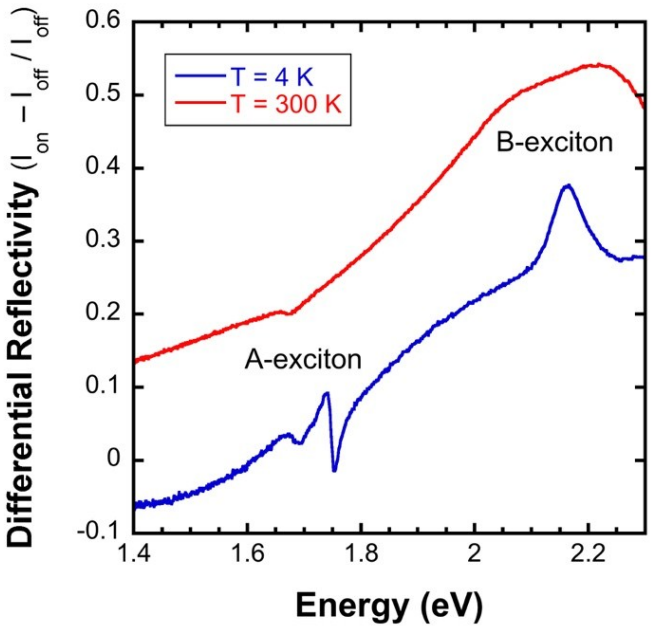

Fig. S2 – Differential reflectivity taken at 4 K and room temperature. The differential reflectivity is defined as the difference between the reflectivity measured with a white light source on the sample and the reflectivity measured just off the sample normalized to the reflectivity off the sample. Differential reflectivity is proportional to absorption and the A-exciton and B-exciton absorption features can be clearly seen in these spectra. For the A-exciton, both the neutral and charged exciton can be resolved at 4 K.

Section 3: **Power Dependence**

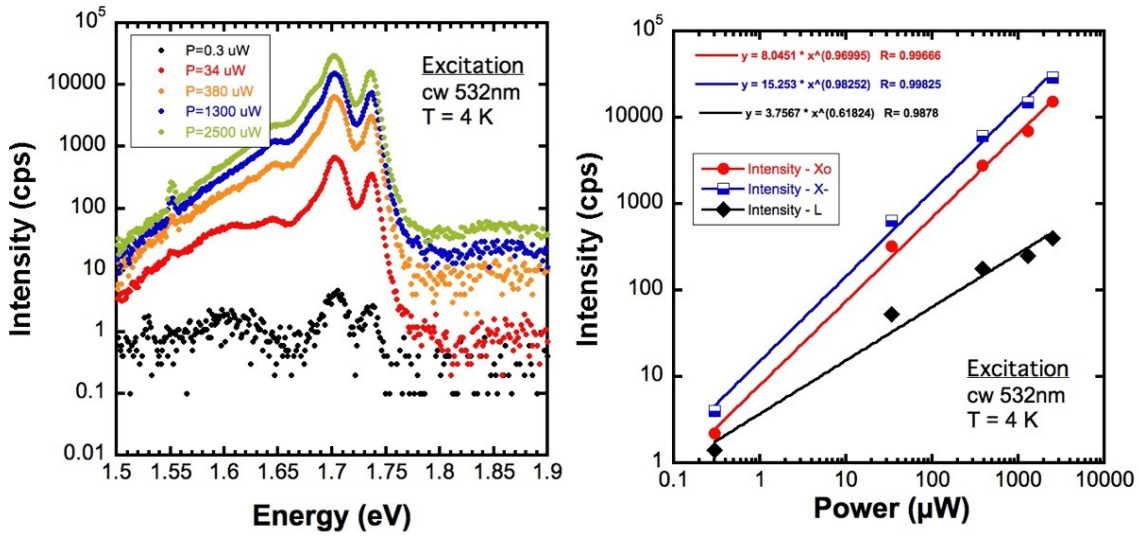

Fig. S3 – PL spectra of WSe_2 collected with cw excitation at 4 K for various powers. The left panel shows the raw spectra and the right panel is a summary of the various peak intensities as a function of power. Note that we are in the linear regime for all cw excitation.

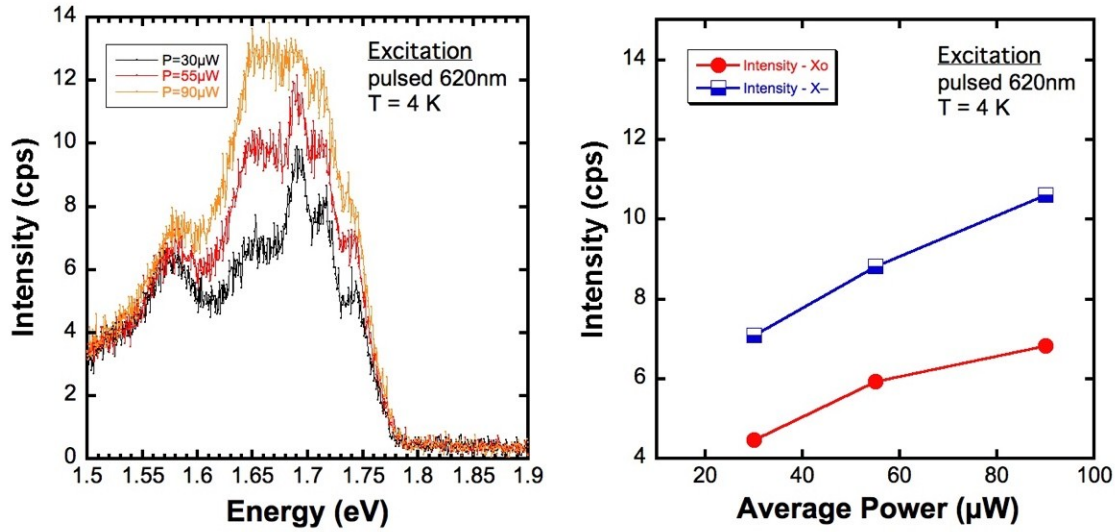

Fig. S4 – PL spectra of WSe_2 collected with pulsed excitation at 4 K for various powers. The left panel shows the raw spectra and the right panel is a summary of the various peak intensities as a function of power. Note the limited range of powers where reproducible PL is accessible using a pulsed laser. Below an average power of 30 μW, the PL intensity is

difficult to observe, above about 90 μW the spectra begin to become permanently affected by the pulse.

Section 4: **Alternate fitting schemes**

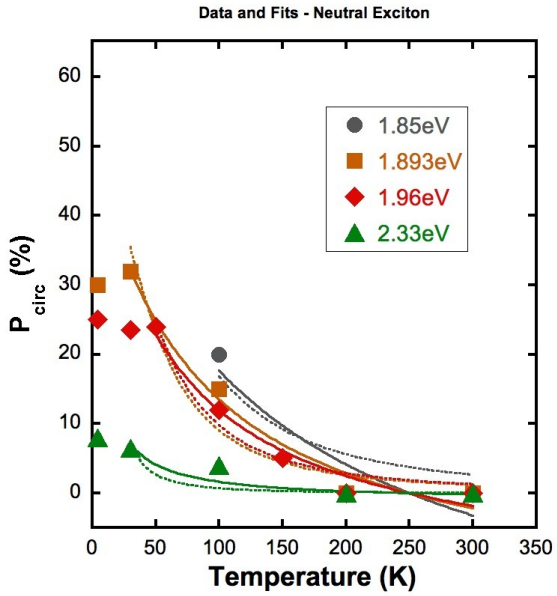

Fig. S5 – Temperature dependence of the circular polarization of the neutral exciton, X^0. The symbols are the data and the lines are fits. The solid line is a fit the model described in the main text where collisional broadening was considered and the dashed line is a fit where simple thermal broadening was used.[3]

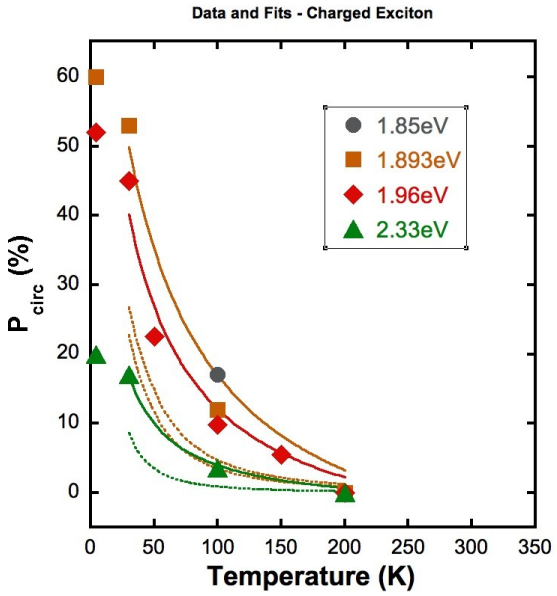

Fig. S6 – Temperature dependence of the circular polarization of the charged exciton, X^T. The symbols are the data and the lines are fits. The solid line is a fit the model described in the main text where collisional broadening was considered and the dashed line is a fit where simple thermal broadening was used.[3]

Section 5: **Raw helicity analyzed PL spectra and fits**

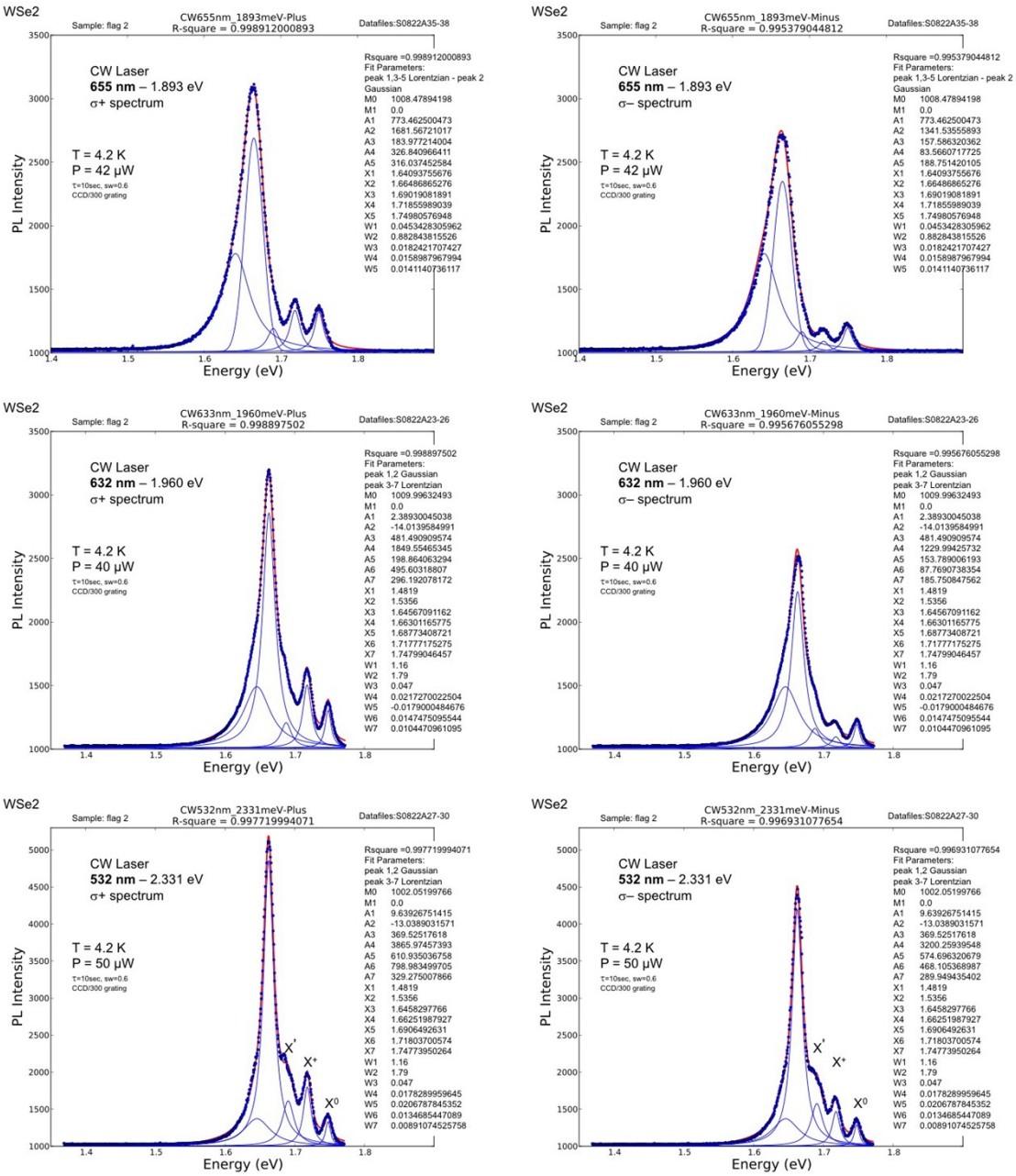

Fig. S7 – Raw data and fits of PL spectra taken with cw excitation at low temperature. Spectra on the left are analyzed for σ+ and spectra on the right are σ–. All peaks are fit in the σ+ spectra and then only the intensity is allowed to vary for the corresponding σ– spectra.

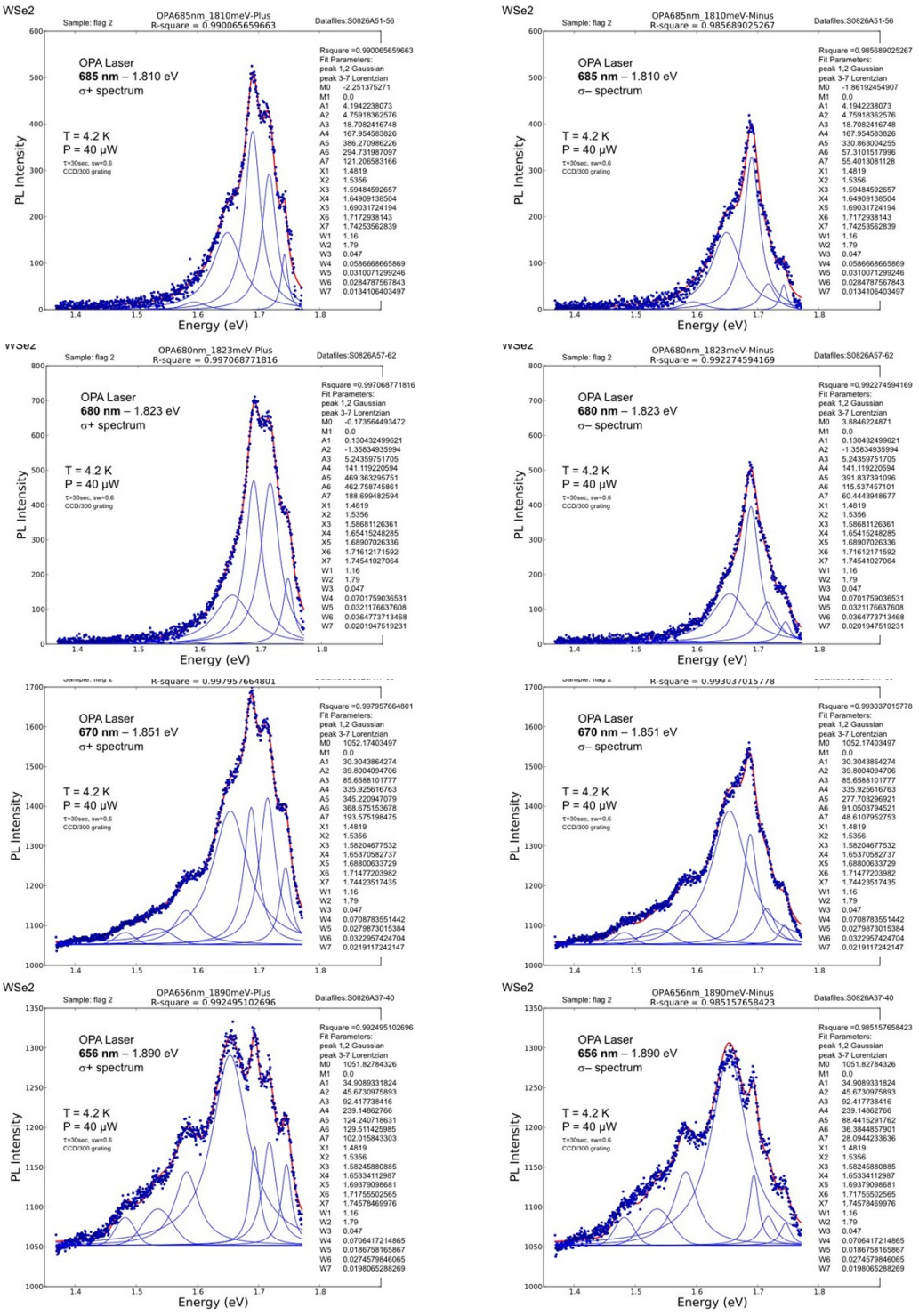

Fig. S8 – Raw data and fits of PL spectra taken with pulsed excitation at low temperature. Spectra on the left are analyzed for σ+ and spectra on the right are σ–. All peaks are fit in the σ+ spectra and then only the intensity is allowed to vary for the corresponding σ– spectra.

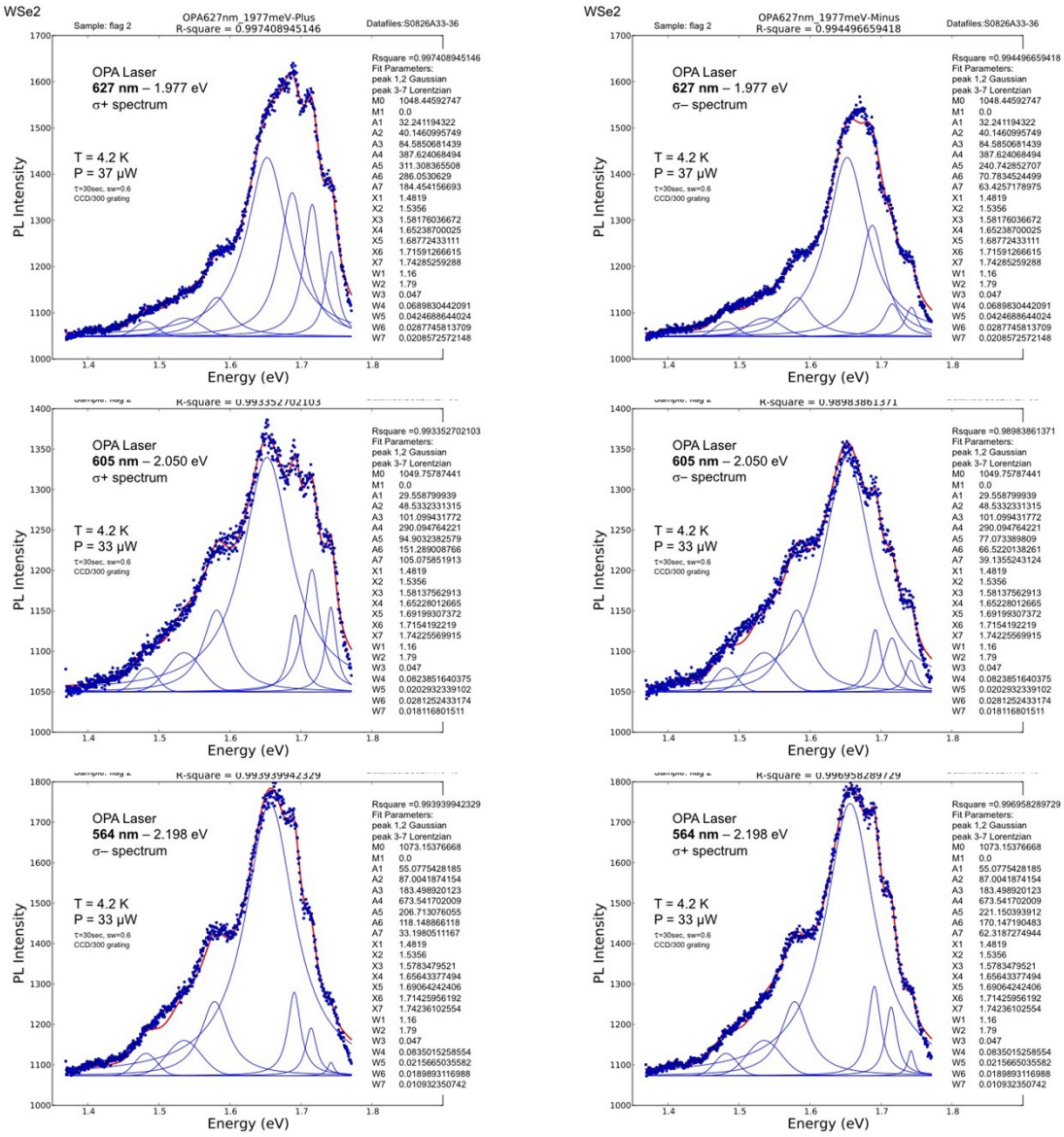

Fig. S9 – Raw data and fits of PL spectra taken with pulsed excitation at low temperature. Spectra on the left are analyzed for σ+ and spectra on the right are σ–. All peaks are fit in the σ+ spectra and then only the intensity is allowed to vary for the corresponding σ– spectra.

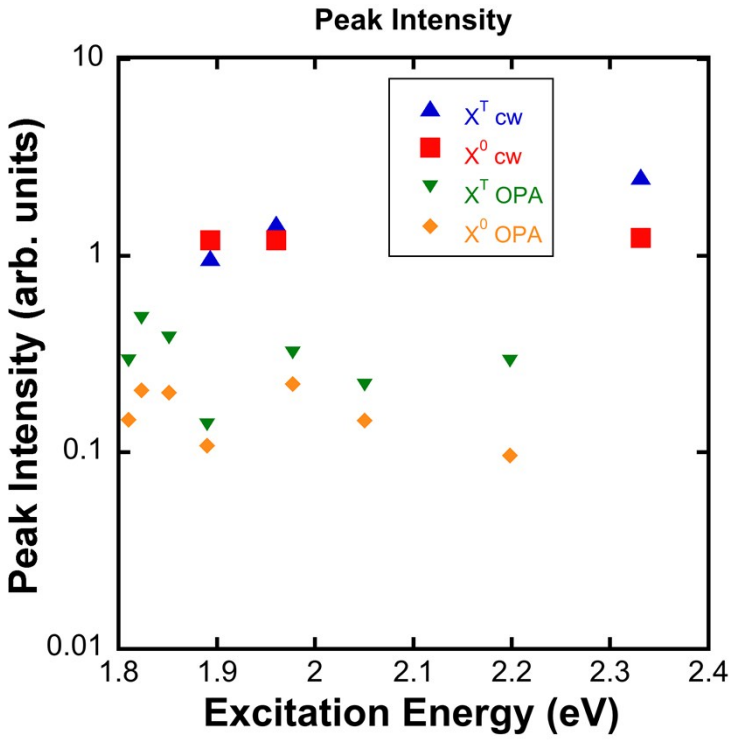

Fig. S10 – Summary of peak intensity vs. Excitation energy resolved for neutral excitons and trions using cw or pulsed excitation. Peak intensities are derived from the fits in figures S3-S6.

Section 6: **Table 1: WSe_2 parameters**

			A-exciton		
Reference	VB Splitting	CB Splitting	X^0	X^T	B-Exciton
This work	0.415 eV	—	1.745 eV	1.717 eV	2.16 eV
[4]-expmt	0.425 eV	—	1.75 eV	1.72 eV	2.17 eV
[5]-expmt	—	—	1.742 eV	1.713 eV	—
[6]-expmt	0.410 eV	—	1.751 eV	1.720 eV	2.16 eV
[7]-expmt	—	—	1.743 eV	1.708 eV	—
[8]-exp	0.480 eV	0.040 eV	1.73 eV	1.70 eV	2.21 eV
[9]-theory	0.466 eV	0.036 eV			
[10]-theory	0.490 eV	0.016 eV			

Section 7: **Rate equations and polarization**

To compute the polarization under pulsed excitation, we solve the following rate equations:

$$\frac{dN_K}{dt} = g - (\alpha + \beta + A)N_K + \beta N_{K'} \quad \text{(S1)}$$

$$\frac{dN_{K'}}{dt} = g' - (\alpha + \beta + A)N_{K'} + \beta N_K \quad \text{(S2)}$$

Here, N_K and $N_{K'}$ are the populations of excitons in the K and K' valleys, g and g' are the generation rates, α is the radiative recombination rate, A is the non-radiative recombination rate, and β is the spin/valley relaxation rate. We assume the pulse is much shorter than any other process and g=g'=0. The solution to these differential equations can be written as

$$N_K(t) = C_1(e^{-(\alpha + A)t} + e^{-(\alpha + A + 2\beta)t}) + C_2(e^{-(\alpha + A)t} - e^{-(\alpha + A + 2\beta)t}) \quad \text{(S3)}$$

$$N_{K'}(t) = C_1(e^{-(\alpha + A)t} - e^{-(\alpha + A + 2\beta)t}) + C_2(e^{-(\alpha + A)t} + e^{-(\alpha + A + 2\beta)t}) \quad \text{(S4)}$$

with constants C_1 and C_2.

At time zero,

$$N_K(t = 0) = 2C_1 \quad \text{(S5)}$$

$$N_{K'}(t = 0) = 2C_2 \quad \text{(S6)}$$

and the initial polarization is given by

$$P_0 = \frac{C_1 - C_2}{C_1 + C_2} \quad \text{(S7)}$$

Assuming all excited carriers decay during the time between pulses, the emission intensities for each polarization are given by the following integrals:

$$I_+/\alpha = \int_0^\infty N_K(t)dt = \frac{C_1 + C_2}{\alpha + A} + \frac{C_1 - C_2}{\alpha + A + 2\beta} \quad \text{(S8)}$$

$$I_-/\alpha = \int_0^\infty N_{K'}(t)dt = \frac{C_1 + C_2}{\alpha + A} + \frac{C_2 - C_1}{\alpha + A + 2\beta} \quad \text{(S9)}$$

Thus the observed polarization is

$$P_{circ} = \frac{I_+ - I_-}{I_+ + I_-} = \frac{\alpha + A}{\alpha + A + 2\beta} \frac{C_1 - C_2}{C_1 + C_2} = \frac{P_0}{1 + 2\beta/(\alpha + A)} \quad \text{(S10)}$$

REFERENCES:

1 H. Sahin, S. Tongay, S. Horzum, W. Fan, J. Zhou, J. Li, J. Wu and F. M. Peeters, *Phys. Rev. B*, 2013, **87**, 165409.

2 P. Tonndorf, R. Schmidt, P. Böttger, X. Zhang, J. Börner, A. Liebig, M. Albrecht, C. Kloc, O. Gordan, D. R. T. Zahn, S. M. de Vasconcellos and R. Bratschitsch, *Opt. Express*, 2013, **21**, 4908–4916.

3 S. Konabe, *Appl. Phys. Lett.*, 2016, **109**, 73104.

4 G. Wang, C. Robert, A. Suslu, B. Chen, S. Yang, S. Alamdari, I. C. Gerber, T. Amand, X. Marie, S. Tongay and B. Urbaszek, *Nat. Commun.*, 2015, **6**, 10110.

5 C. R. Zhu, K. Zhang, M. Glazov, B. Urbaszek, T. Amand, Z. W. Ji, B. L. Liu and X. Marie, *Phys. Rev. B*, 2014, **90**, 161302(R).

6 G. Wang, L. Bouet, D. Lagarde, M. Vidal, A. Balocchi, T. Amand, X. Marie and B. Urbaszek, *Phys. Rev. B*, 2014, **90**, 75413.

7 Y. You, X.-X. Zhang, T. C. Berkelbach, M. S. Hybertsen, D. R. Reichman and T. F. Heinz, *Nat. Phys.*, 2015, **11**, 477–481.

8 Z. Wang, L. Zhao, K. F. Mak and J. Shan, *Nano Lett.*, 2017, **17**, 740–746.

9 G.-B. Liu, W.-Y. Shan, Y. Yao, W. Yao and D. Xiao, *Phys. Rev. B*, 2013, **88**, 85433.

10 J. P. Echeverry, B. Urbaszek, T. Amand, X. Marie and I. C. Gerber, *Phys. Rev. B*, 2016, **93**, 121107.